Chemical Science

EDGE ARTICLE

View Article Online
View Journal | View Issue

Cite this: *Chem. Sci.*, 2016, **7**, 1212

Oxidation triggers extensive conjugation and unusual stabilization of two di-heme dication diradical intermediates: role of bridging group for electronic communication†

Debangsu Sil, Soumyajit Dey, Amit Kumar, Susovan Bhowmik and Sankar Prasad Rath*

MauG is a diheme enzyme that utilizes two covalently bound c-type hemes to catalyse the biosynthesis of the protein-derived cofactor tryptophan tryptophylquinone. The two hemes are physically separated by 14.5 Å and a hole-hopping mechanism is proposed in which a tryptophan residue located between the hemes undergoes reversible oxidation and reduction to increase the effective electronic coupling element and enhance the rate of reversible electron transfer between the hemes in bis-Fe(IV) MauG. The present work describes the structure and spectroscopic investigation of 2e-oxidations of the synthetic diheme analogs in which two heme centers are covalently connected through a conjugated ethylene bridge that leads to the stabilization of two unusual *trans* conformations (*U* and *P*′ forms) with different and distinct spectroscopic and geometric features. Unlike in MauG, where the two oxidizing equivalents are distributed within the diheme system giving rise to the bis-Fe(IV) redox state, the synthetic analog stabilizes two ferric hemes, each coupled with a porphyrin cation radical, a scenario resembling the binuclear dication diradical complex. Interestingly, charge resonance-transition phenomena are observed here both in 1e and 2e-oxidised species from the same system, which are also clearly distinguishable by their relative position and intensity. Detailed UV-vis-NIR, X-ray, Mössbauer, EPR and ^{1}H NMR spectroscopic investigations as well as variable temperature magnetic studies have unraveled strong electronic communications between two porphyrin π-cation radicals through the bridging ethylene group. The extensive π-conjugation also allows antiferromagnetic coupling between iron(III) centers and porphyrin radical spins of both rings. DFT calculations revealed extended π-conjugation and H-bonding interaction as the major factors in controlling the stability of the conformers.

Received 21st August 2015
Accepted 26th October 2015

DOI: 10.1039/c5sc03120f

www.rsc.org/chemicalscience

Introduction

Metalloporphyrin π-cation radicals are of immense interest due to their occurrence as intermediates in the catalytic cycle of many heme containing enzymes, *e.g.*, peroxidases,[1] catalases,[2] cytochrome P450 [1a,3] *etc.*, and their photosynthetic reaction center.[4] In spite of the common active intermediates, the reactivity differs from enzyme to enzyme. The extent of coupling between metal center and porphyrin π-cation radical may be linked to the various activities in the heme enzymes, and this has therefore led to the study of metalloporphyrin π-cation radicals and mixed valence π-cation radicals (where one electron is removed per two porphyrin rings).[5,6]

Numerous diheme enzymes such as MauG[7,8] and bacterial diheme cytochrome c peroxidases (bCcP)[9] serve as active catalysts in various important chemical transformations in biology. For instance, bCcP mediates peroxidase activity, whereby it transfers the oxidizing equivalents from H_2O_2 to cytochrome c or other small redox proteins.[9] MauG (Fig. 1) is a terminal enzyme involved in the biosynthesis of the catalytic tryptophan tryptophylquinone (TTQ) cofactor of methylamine dehydrogenase (MADH). Although the two heme units are physically separated in both enzymes, they share electrons efficiently behaving as a single diheme unit rather than as independent heme centers. A tryptophan residue is, however, positioned in between two heme centers and has been proposed to act as a bridge in order to promote the electronic communication between the heme centers.[7–9]

High-valent Fe(IV)=O intermediates are frequently invoked in the catalytic cycles of Fe-dependent oxidizing enzymes.[1–3] In heme-dependent enzymes, the two-electron oxidized intermediate (compound I) consists of an Fe(IV) species ($S = 1$) coupled to an organic radical ($S = 1/2$) that is located on the porphyrin

Department of Chemistry, Indian Institute of Technology Kanpur, Kanpur-208016, India. Fax: +91-512-259 6806. E-mail: sprath@iitk.ac.in

† Electronic supplementary information (ESI) available: Text, figures and tables depicting synthetic procedures, detailed experimental procedures, characterisation data including UV-vis-NIR, FT-IR, DFT. CCDC 1052187 and 1052188. For ESI and crystallographic data in CIF or other electronic format see DOI: 10.1039/c5sc03120f

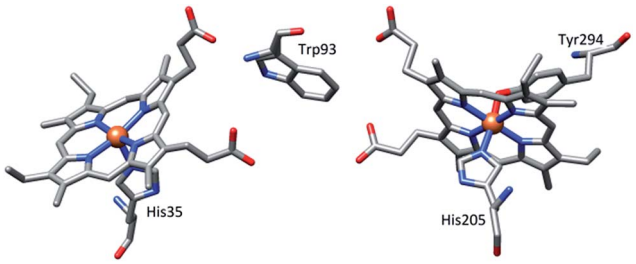

Fig. 1 Relative orientation of hemes and the intervening tryptophan residue in MauG (PDB ID code 3L4M).[7a]

ring/axial ligand or a nearby amino acid residue (compound ES). In MauG, however, two oxidizing equivalents derived from H_2O_2 are distributed within the diheme system as two positive charges, giving rise to a bis-Fe(IV) redox state (Scheme 1) in which one heme is present as Fe(IV)=O and the other as Fe(IV) with axial histidine and tyrosine ligation.[8] As the two hemes are physically separated by 14.5 Å, a hole-hopping mechanism was proposed wherein the tryptophan residue reversibly oxidized and reduced in order to boost the effective electronic coupling element and magnify the rate of electron transfer between the heme centers in the bis-Fe(IV) MauG.[8]

The electronic communication between the porphyrin moieties in the ground and/or excited state can be facilitated by using covalently connected linkers in conjugation with porphyrin rings. In this context, a large number of porphyrin dimers connected *via* conjugated linkers, *viz.* alkene, alkyne, imino, and azo bridges, have been studied due to their unique optical properties.[10] Our recent efforts have been directed towards exploring the role of intermacrocyclic interactions in modulating various properties, *viz.* redox potential, spin state *etc.*[11] However, interactions between a pair of porphyrin π-cation radicals connected through a linker remain unexplored.

In the present study, we have made synthetic analogs of the diheme centers of MauG in which two porphyrin rings have been covalently connected through a conjugated but rigid ethylene bridge which would separate the two macrocycles to the furthest extent. Step-wise oxidations up to two oxidizing equivalents have been performed using chemical oxidants. Unlike the bis-Fe(IV) state as obtained in MauG, the two electron oxidized complex stabilizes two ferric hemes, each coupled with a porphyrin cation radical, a scenario resembling the binuclear dication diradical complex. This work describes an alternative mechanism to store two oxidizing equivalents above the ferric state in dihemes. Spectroscopic investigations have unraveled strong electronic communications between two porphyrin π-cation radicals *via* the ethylene bridge which eventually alter the nature of such bridge. The extensive π-conjugation also allows antiferromagnetic coupling between iron(III) centers and porphyrin radical spins of both rings. DFT calculations have been employed which further support our spin-coupling model as obtained from the magnetic measurements and also provide insight into the preferential stabilization of various geometrical conformers under certain conditions.

In earlier work on monomeric metalloporphyrin π-cation radicals, spin coupling between the metal ion and the oxidized porphyrin ring in a number of derivatives that differed in metal ion, axial ligation, and/or porphyrin ligand were investigated.[5,6] The inter-ring coupling was found to be closely related only to the degree of the ring overlap. In the present investigation, however, the inter-ring coupling between two monomeric Fe(III) porphyrin π-cation radicals has been demonstrated to occur only through the bridge although they are widely separated in space.

Result and discussion

Dichlorodiiron(III) ethylene bridged octaethyl porphyrin dimers have been synthesized both in *cis* (*cis*-**1**) and *trans* (*trans*-**1**) isomers using the procedures reported earlier.[11j,12] Oxidation of these complexes has been performed in a step-wise manner using chemical oxidants and monitored using UV-vis-NIR spectroscopy. Scheme 2 shows the synthetic outline and list of diheme dication diradical intermediates reported here along with the abbreviations used.

Fig. 2 shows the UV-visible spectral changes upon step-wise oxidations of *cis*-**1** using $Fe(ClO_4)_3$ as an oxidant. Gradual addition of a CH_3CN solution of $Fe(ClO_4)_3$ as an oxidizing agent in up to one equivalent to a dichloromethane solution of *cis*-**1** leads to a sharp decrease in the Soret band intensity at 390 nm along with the appearance of a low energy band at 989 nm, which is characteristic of the intra-valence charge transfer obtained due to the formation of a mixed-valence π-cation radical dimer.[6,13] The absorbance of the 989 nm band has showed a linear dependence on the concentration, ruling out the possibility of intermolecular dimerization as its origin.[6] On further addition of the $Fe(ClO_4)_3$ solution in up to two

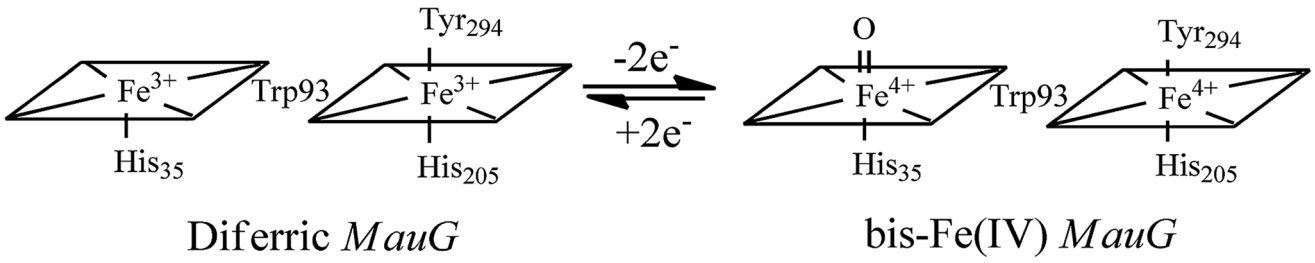

Scheme 1 Conversion of the hemes of MauG from diferric to bis-Fe(IV) redox state.[8]

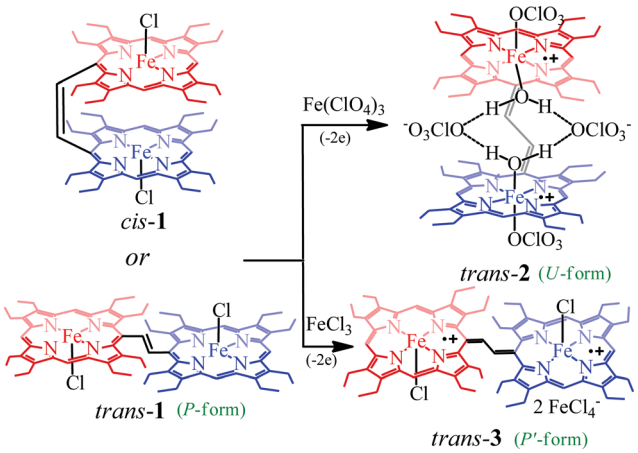

Scheme 2 Synthetic outline.

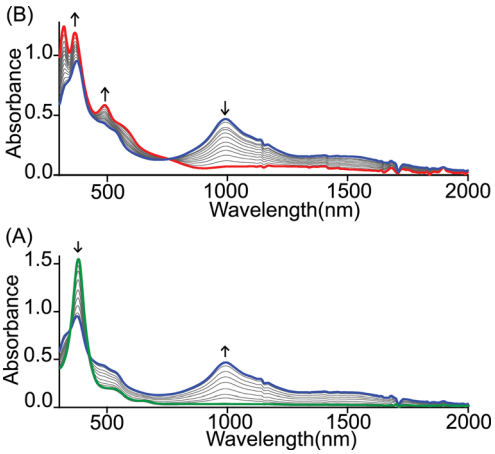

Fig. 3 UV-vis-NIR (in CH_2Cl_2 at 295 K) spectral change of 2.1×10^{-5} (M) solution of *cis*-**1** upon gradual addition of (A) 0 to 2.0 and (B) 2.0 to 4.0 eq. of $FeCl_3$.

equivalents, the Soret band at 390 nm decreases gradually again along with the appearance of two new bands at 326 and 477 nm, while the intensity of the absorbance at 989 nm decreases with the appearance of a new broad band near 1150 nm. The 2e-oxidized complex thus obtained has been isolated in the solid state as a dication diradical species (*trans*-**2**) in good yields and has been structurally characterized. Further addition of the oxidant showed no observable change in the absorption spectra.

Similar spectral changes have also been obtained during the oxidation of *cis*-**1** when $FeCl_3$ was used as an oxidant (Fig. 3). Upon one-electron oxidation, a sharp decrease in the Soret band intensity at 390 nm has been observed along with the appearance of a low energy band at 989 nm due to the formation of a mixed-valence π-cation radical dimer. Upon addition of the $FeCl_3$ solution in up to four equivalents, the Soret band at 390 nm increased gradually and underwent a blue shift to 365 nm along with the appearance of two new bands at 317 and 488 nm in the UV-visible regions. In the NIR region, the intensity of the absorbance at 989 nm decreases while a broad band near 1210 nm appears. The two-electron oxidized complex thus obtained has also been isolated as a dication diradical species (*trans*-**3**) in the solid state and has been structurally characterized. The absorption spectrum of *trans*-**3** displays a Soret band at 365 nm, two new bands at 317 and 488 nm, and a broad NIR band near 1210 nm. *Trans*-**1** also produces similar spectral changes upon oxidation with $Fe(ClO_4)_3/FeCl_3$ leading to the formation of *trans*-**2**/**3**, respectively (Fig. S1 and S2†). Gradual addition of an

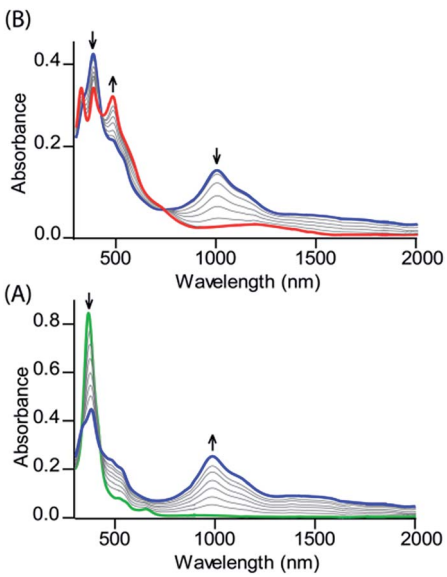

Fig. 2 UV-vis-NIR (in CH_2Cl_2 at 295 K) spectral change of 1.2×10^{-5} (M) solution of *cis*-**1** upon gradual addition of (A) 0 to 1.0 eq. and (B) 1.0 to 2.0 eq. of $Fe(ClO_4)_3$.

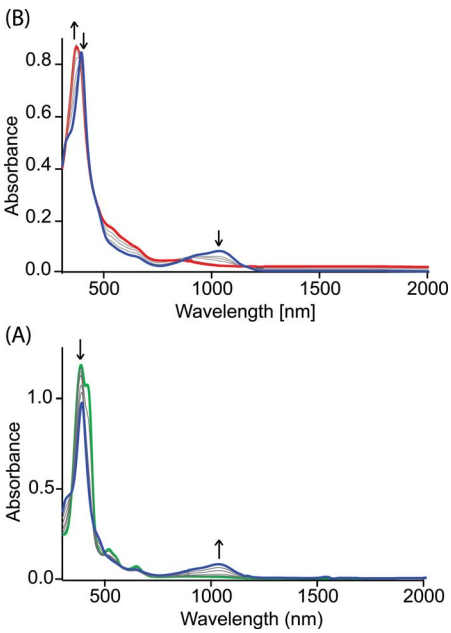

Fig. 4 UV-vis-NIR spectral change (in CH_2Cl_2 at 295 K) of 1.4×10^{-5} (M) solution of **4** (green line) upon gradual addition of (A) 0 to 1.0 and (B) 1.0 to 2.0 eq. of $Fe(ClO_4)_3$.

acetonitrile solution of $Fe(ClO_4)_3$ to a CH_2Cl_2 solution of *trans*-**1** at −40 °C (Fig. S3†) also showed similar spectral changes as observed at room temperature.

Fig. 4 shows the UV-visible spectral change upon gradual addition of a CH_3CN solution of $Fe(ClO_4)_3$ into a CH_2Cl_2 solution of 1,2-bis[(chloro){5-(2,3,7,8,12,13,17,18-octaethylporphyrinato)}iron(III)]ethane, **4** (Chart 1), which is a highly flexible ethane-bridged analog of **1**. Upon 1e-oxidation, the intensity of the Soret band decreases slightly along with a small blue-shift while a low-intense NIR band at 1100 nm is observed which, however, upon 2e-oxidation disappears completely.

It is interesting to compare the UV-vis-NIR spectra of 2e-oxidized complexes reported in Fig. 5. The absorption bands in the 480–500 nm, 600–900 and 1100–1300 nm regions, which are observed in both *trans*-**2** and *trans*-**3**, are absent completely in the 2e-oxidized product of **4** and are, therefore, attributed to the extensive conjugation between two porphyrin π-cation radicals (*vide infra*) in the former complexes. The intensity of the Soret band has also been drastically reduced in *trans*-**2** and *trans*-**3** (as compared to the 2e-oxidized product of **4**) which is suggestive of reduced aromaticity of the porphyrin rings in the complexes because of conjugation (*vide infra*).[10c]

The broad NIR band that is observed at 1150 and 1210 nm for *trans*-**2** and *trans*-**3** can be attributed to the charge resonance (CR) stabilization of the spins and charges in the binuclear dication diradical complex. The CR stabilization energy (ΔE_{CR}) originates from exchange interactions between the molecular orbitals of each monomer and subsequent delocalization of the spin and charge over a greater number of atoms.[6b,8,13] During the 1e-oxidation process (*vide supra*), a broad and slightly more intense NIR band at ~1000 nm was obtained which is also attributed to charge resonance phenomena of the mixed-valence π-cation radical dimer.[6,8] Interestingly, CR-transition phenomena are observed here in both 1e and 2e-oxidized complexes from the same system while the NIR bands are also clearly distinguishable by their relative position and intensity. Despite the inherent energy penalty caused by the electrostatic repulsion in the dication complex, the CR stabilization energy of the dication diradical species is larger than that of the mixed-valence π-cation radical dimer of the same system, which results in a blue-shift of the CR band.[6b,8,13] In contrast, a red-shift of CR bands is observed when moving our attention from 1e to 2e-oxidation, and this is due to multiple factors related to charge delocalization through bridging ligand, intramolecular coupling between iron–radical and radical–radical spins (*vide infra*) *etc.* Through the bridging ethylene group, both porphyrin macrocycles exhibit substantial conjugation which eventually

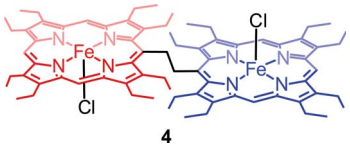

4

Chart 1 1,2-Bis[(chloro){5-(2,3,7,8,12,13,17,18-octaethylporphyrinato)}iron(III)]ethane, **4**.

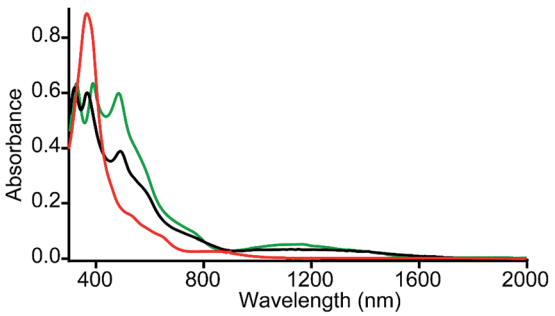

Fig. 5 UV-vis-NIR spectra (in CH_2Cl_2 at 295 K) of *trans*-**2** (green line), *trans*-**3** (black line) and 2e-oxidized product of **4** (red line).

alters the nature of the bridge (ethylene to *exo*-methylene connectivity) resulting the stabilization of two unusual *trans* conformers (*U* and *P*′ type, *vide infra*). Moreover, the NIR bands in the absorption spectra of *trans*-**2** and *trans*-**3** are found to be linearly correlated with the concentration (Fig. 6 and S4†). Such Beer's law concentration dependence further supports the intramolecular origin of the CR bands.[5,6] The MauG-catalyzed reaction proceeds through a bis-Fe(IV) intermediate which has been shown to exhibit CR phenomena. The bis-Fe(IV) state is an electronic equivalent of two Fe(III)porphyrin π-cation radicals with each radical spin coupled to the Fe(III) atom. Although there is large separation between two heme centers, such spin/charge resonance stabilization is facilitated by the presence of a Trp93 residue which bridges between heme centers.[8]

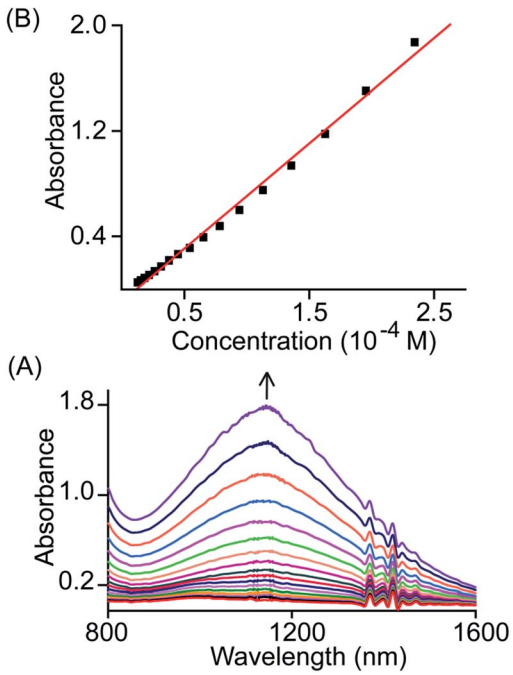

Fig. 6 (A) Gradual change in the absorbance of the NIR band (in CH_2Cl_2 at 295 K) of *trans*-**2** with change in concentration and (B) plot of absorbance of the NIR band as a function of concentration.

The formation of porphyrin π-cation radicals is often signalled by strong IR bands.[5,6] Fig. S5† displays selected portions of the IR spectra of *trans*-**2** and *trans*-**3** along with their unoxidized analogs, *cis*-**1** and *trans*-**1**. The oxidized species, *trans*-**2** and *trans*-**3**, show π-cation radical IR marker bands at 1546, 1598 and 1544, 1595 cm^{-1}, which are absent in the unoxidized complexes. The ~1550 cm^{-1} band is due to the asymmetric C_α–C_{meso} stretching mode while the ~1600 cm^{-1} band is due to the C_β–C_β stretch. Similar IR marker bands have also been reported earlier in octaethylporphyrinate and β-alkyl substituted porphyrinate π-cation radical derivatives.[5,6] Thus, the IR spectral data further confirms *trans*-**2** and *trans*-**3** as porphyrin π-cation radicals. The molar conductances at 295 K of *trans*-**2** (41 Ω^{-1} cm^2 mol^{-1}) and *trans*-**3** (42 Ω^{-1} cm^2 mol^{-1}) in dichloromethane are similar to the values observed for 1 : 2 electrolytes in solution.[14]

Crystallographic characterizations

Dark needle crystals of *trans*-**2** and *trans*-**3** were grown *via* slow diffusion of hexane into chloroform and dichloromethane solutions of the complexes in air at room temperature. Perspective views of the complexes along with the molecular packing are depicted in Fig. 7 and 8. Table 1 lists the crystallographic data and data collection parameters of the complexes reported here. Both molecules crystallize in the monoclinic crystal system, however, *trans*-**2** does so with a *P*2/*c* space group

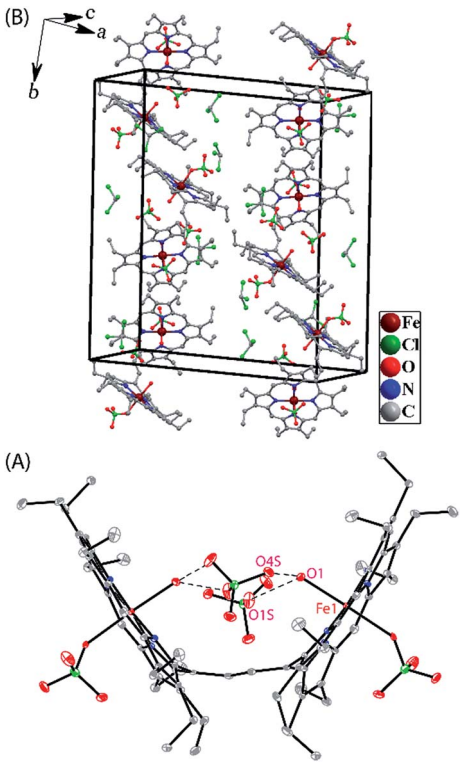

Fig. 7 (A) A perspective view (at 100 K) of *trans*-**2** showing 50% thermal contours (H atoms have been omitted for clarity). (B) Diagram illustrating the packing of *trans*-**2** in the unit cell (H-atoms have been omitted for clarity).

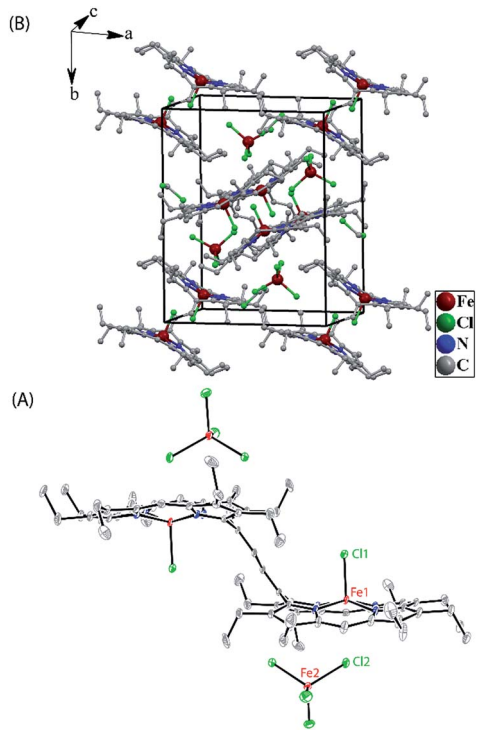

Fig. 8 (A) A perspective view (at 100 K) of *trans*-**3** showing 50% thermal contours (H atoms have been omitted for clarity). (B) Diagram illustrating the packing of *trans*-**3** in the unit cell (H-atoms have been omitted for clarity).

while *trans*-**3** crystallizes with a $P2_1/n$ space group. Iron centers are in six-coordinate geometry with water and perchlorate axial ligands for *trans*-**2** and five-coordinate geometry with chloride ion as axial ligand in *trans*-**3**. The porphyrin cores of the complexes showed considerable doming. Table S1† shows the selected bond distances and angles while Table 2 compares the structure and geometrical parameters of *trans*-**2** and *trans*-**3** along with their unoxidized complex, *trans*-**1**.

The average Fe–N_p distances in the two types of complexes are very different: 2.027(4) and 2.034(4) Å for cores I and II in *trans*-**2** and 2.045(3) Å in *trans*-**3** which are characteristic of admixed high-spin and high-spin states of iron.[11,15,16] The Fe–Cl bond distance of 2.2249(11) Å in *trans*-**3** is shorter than the 2.241(2) Å observed in the unoxidized complex, *trans*-**1**. The slight contraction of the Fe–Cl bond distance is consistent with the increased positive charge in the oxidized complex. The displacement of iron(III) from the mean plane of the $C_{20}N_4$ porphyrinato core (Fe···Ct_p) in *trans*-**3** is 0.50 Å which is slightly larger than the 0.48 Å observed in *trans*-**1**.[11h] However, the Fe···Ct_p distances in the six-coordinate complex, *trans*-**2**, are 0.10 and 0.04 Å for cores I and II, respectively, and iron is displayed in the direction of the axial H_2O ligand. Although the ligand field strength of ClO_4^- is greater than for H_2O according to the magnetochemical series,[17] this is outweighed by the strong H-bonding interactions between the ligated H_2O and ClO_4^- counterions which hold the structure in place.

Table 1 Crystallographic data and data collection parameters

	trans-**2**	*trans*-**3**
Formula	$C_{78}H_{96}Cl_{16}Fe_2N_8O_{18}$	$C_{76}H_{92}Cl_{14}Fe_4N_8$
T (K)	100(2)	100(2)
Formula weight	2112.52	1837.27
Crystal system	Monoclinic	Monoclinic
Space group	$P2/c$	$P2_1/n$
a, Å	31.467(5)	15.165(5)
b, Å	9.589(5)	18.236(5)
c, Å	30.770(5)	15.623(5)
α, deg	90	90
β, deg	91.556(5)	103.044(5)
γ, deg	90	90
V, Å^3	9281(5)	4209(2)
Z	4	2
d_{calcd}, g cm^{-3}	1.512	1.450
μ, mm^{-1}	0.842	1.166
F(000)	4352	1892
Crystal size	0.26 × 0.20 × 0.16 mm^3	0.22 × 0.16 × 0.12 mm^3
No. of unique data	17277	7814
Completeness to theta = 25.00°	99.9%	99.9%
No. of parameters refined	1166	496
GOF on F^2	1.031	1.032
R_1[a] [$I > 2\sigma(I)$]	0.0679	0.0489
R_1[a] (all data)	0.1108	0.0680
wR_2[b] (all data)	0.1791	0.1332
Largest diff. peak and hole	1.324 and −1.101 e Å^{-3}	0.910 and −0.745 e Å^{-3}

[a] $R_1 = \frac{\sum||F_o| - |F_c||}{\sum|F_o|}$. [b] $wR_2 = \sqrt{\frac{\sum[w(F_o^2 - F_c^2)^2]}{\sum[w(F_o^2)^2]}}$.

Table 2 Selected structural parameters

		trans-**2**		
	trans-**1**[a]	Molecule-I	Molecule-II	*trans*-**3**
Fe–N_p (Å)[b]	2.055(6)	2.027(4)	2.034(4)	2.045(3)
Fe–O(H_2) (Å)	—	2.093(3)	2.095(3)	—
Fe–O(ClO_3) (Å)	—	2.187(3)	2.178(3)	—
Fe–Cl (Å)	2.241(2)	—	—	2.2249(11)
Δ_{24}^{Fe} (Å)[c]	0.48	0.10	0.04	0.50
Δ_{24} (Å)[d]	0.21	0.20	0.16	0.26
Fe···Fe (Å)	9.84	8.33	8.31	9.32
Θ (°)[e]	65.79	56.59	57.13	55.82
C20–C37 (Å)	1.478(9)	1.374(6)	1.371(6)	1.364(4)
C37–C37A (Å)	1.312(13)	1.435(9)	1.433(9)	1.432(7)

[a] Taken from ref. 11*h*. [b] Average value. [c] Displacement of iron from the least-squares plane of the $C_{20}N_4$ porphyrinato core. [d] Average displacement of atoms from the least-squares plane of $C_{20}N_4$ porphyrinato core. [e] Inter-planar angle between the least-squares plane of the $C_{20}N_4$ porphyrinato core and the C_4 plane of the bridging ethylene group (see Fig. 9A).

The most striking feature of *trans*-**2** is the unusual bowl shaped conformation (*U*-form) of the bisporphyrin unit which is stabilized by four H-bonding interactions [O···O: 2.761(5), 2.931(5), 2.926(5) and 2.767(5) Å] between the coordinated H_2O molecules and the ClO_4^- counterions. The inter-planar angles (Θ) between the plane of the ethylene bridge and that of the porphyrin rings are 56.59° and 57.13° in *trans*-**2** (Table 2) as compared to 65.79° obtained for *trans*-**1**. Although steric interactions with the β-ethyl substituents in *trans*-**1** tend to prevent a coplanar arrangement of the porphyrin rings and the ethylene bridge, the extensive conjugation in the dication diradical species (*trans*-**2**) imposes a better coplanarity. The extended conjugation between two porphyrin units through the bridging ethylene moiety is manifested in the alteration of the C20–C37 and C37–C37A bond distances. The C20–C37 bond lengths of 1.374(6) (molecule-I) and 1.371(6) Å (molecule-II) in *trans*-**2** are close to the C=C distance, while the C37–C37A bond lengths of 1.435(9) (molecule-I) and 1.433(9) Å (molecule-II) become close to that of a C–C single bond. This results in a situation where the ethylene bridge (C–CH=CH–C) transforms into an *exo*-methylene (C=CH–CH=C) connectivity between two porphyrin rings (Fig. 9B).

The X-ray structure of *trans*-**3** is similar to that of *trans*-**1** in terms of relative orientation of the two porphyrin rings; however, they differ remarkably in several structural and geometrical parameters. The C20–C37 and C37–C37A bond distances of 1.364(4) and 1.432(7) Å and the inter-planar angle (Θ) of 55.82° in *trans*-**3** are similar to those of *trans*-**2**, which is indicative of strong intramolecular electronic conjugation between the two rings through the ethylene bridge. The alteration of the C20–C37 and C37–C37A bond distances leads to a single bond connecting two *exo*-methylene groups at C20 of

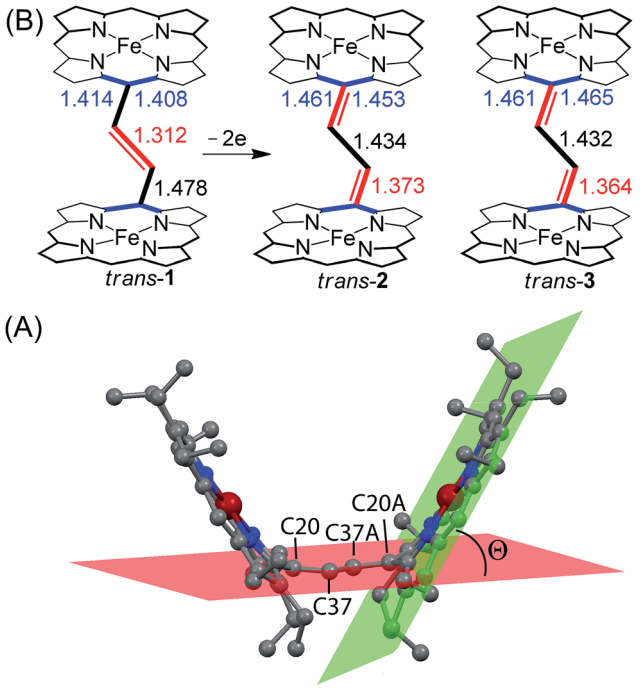

Fig. 9 (A) Diagram illustrating the angle Θ between the least-squares plane of $C_{20}N_4$ porphyrinato core (green) and the calculated C_4 plane of the bridging ethylene group (red) of *trans*-**2** as a representative case. (B) Selected bond distances (in Å) between oxidized and unoxidized complexes have been compared. H-atoms, axial ligands and counterions have been omitted for clarity.

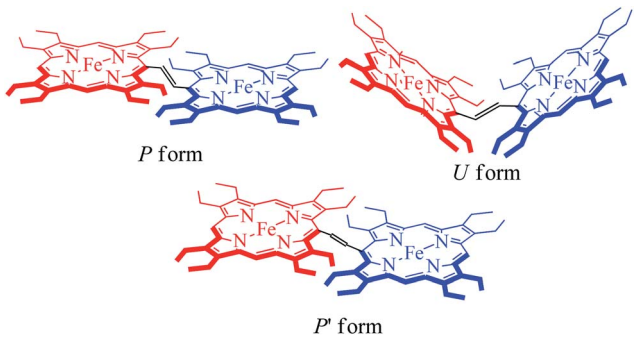

Scheme 3 Different conformations of *trans* ethylene-bridged Fe(III) bisporphyrin framework.

the two porphyrin rings. Scheme 3 describes the three possible conformations for the *trans* isomer. In one conformation, both porphyrins are completely orthogonal to the alkene (normal *P*-type), while in other two the macrocycles are almost in plane with the bridged ethylene moiety and the rings are either cofacial (*U*-type) or anti (*P*′-type) with respect to each other.[10f,g] The 2e-oxidized complexes, *trans*-**2** and *trans*-**3**, do not stabilize in the normal *P*-type conformation but in the unusual *U* and *P*′-conformations, which facilitates extended conjugation between the two radical cores. This is the first structural evidence of the *U* and *P*′ forms in β-alkyl substituted bisporphyrins. Although the *P*′-form has been previously observed in a few β-

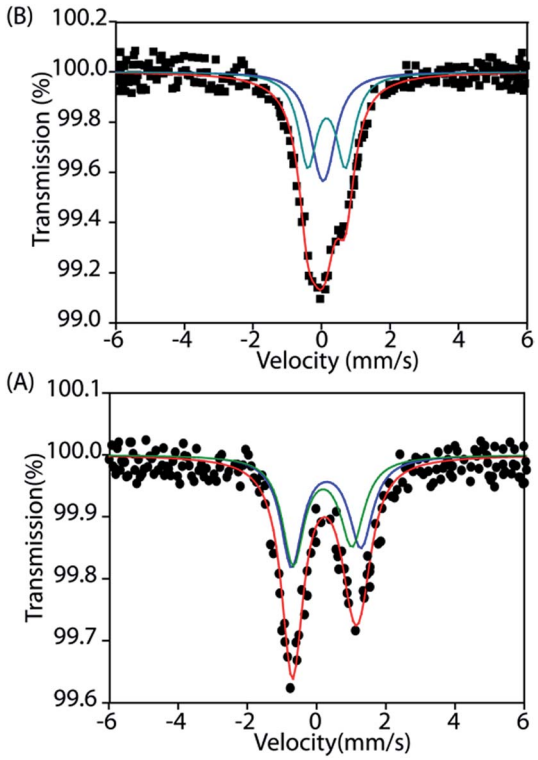

Fig. 10 Mössbauer spectra of (A) *trans*-**2** and (B) *trans*-**3** at 295 K.

unsubstituted bisporphyrins,[10c–e] no such conformers could be stabilized in β-alkyl substituted bisporphyrins due to steric interactions from the extreme closeness of the alkyl groups.

Mössbauer

To gain further insight into the electronic structure, we studied both *trans*-**2** and *trans*-**3** by Mössbauer spectroscopy. Fig. 10 shows the solid state Mössbauer spectra of the oxidized complexes at 295 K. The Mössbauer spectra provide compelling evidence that oxidation has occurred at the porphyrin ring only. *trans*-**2** shows the presence of two quadrupole-split doublets [δ (ΔE_q): 0.39 (2.0) and 0.33 (1.7) mm s^{-1}], suggesting the presence of two admixed high-spin Fe(III) centers[11,15,16] in the molecule as also observed in the X-ray structure (*vide supra*). In contrast, *trans*-**3** displays two quadrupole-split doublets, one of which has parameters comparable to the tetrachloroferrate anion[18a] [δ = 0.19 mm s^{-1}, ΔE_q = 0.23 mm s^{-1}] while the other represents a high-spin iron(III) centre [δ = 0.29 mm s^{-1}, ΔE_q = 1.1 mm s^{-1}].

Magnetic measurements

The magnetic susceptibility of *trans*-**2** and *trans*-**3** has been measured between 5 to 300 K using two different applied magnetic fields of 0.1 and 1 T which provide very similar results.

In an attempt to obtain a quantitative description of the spin–spin interaction that led to the observed magnetic moment, the magnetic susceptibility data were fitted using the software PHI.[19] Acceptable fits (Fig. 11) have been obtained using a model which included three pairs of interactions: (a)

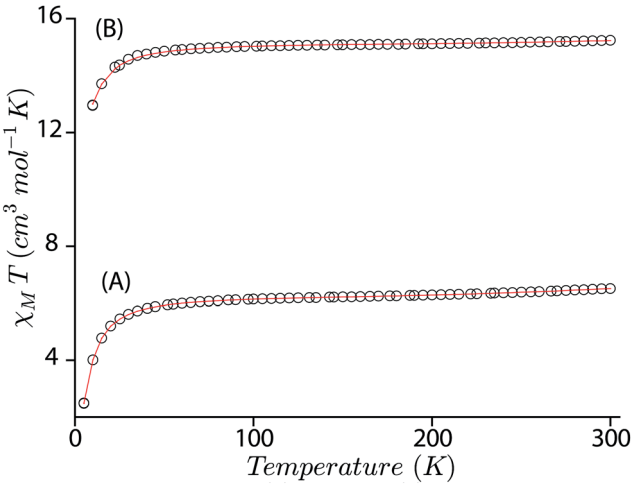

Fig. 11 $X_M T$ *versus* *T* plots for (A) *trans*-**2**, and (B) *trans*-**3**. The solid lines are best fits using the values given in the text.

intramolecular coupling between the iron and π-cation radical spin (J_{Fe-r}), (b) intramolecular coupling between two iron spins (J_{Fe-Fe}), and (c) intramolecular coupling between the two radical spins of the bisporphyrin (J_{r-r}). Each iron(III) center was treated as high spin ($S = 5/2$) with a *g* value set at 2.0 and the presence of small residual mononuclear iron(III) impurities was also taken into consideration. The parameters obtained from the fits are: $J_{Fe-r} = -124.36\ cm^{-1}$, $J_{Fe-Fe} = -0.05\ cm^{-1}$, $J_{r-r} = -16.67\ cm^{-1}$, $D = 4.0\ cm^{-1}$ for *trans*-**2**, $J_{Fe-r} = -149.88\ cm^{-1}$, $J_{Fe-Fe} = -0.13\ cm^{-1}$, $J_{r-r} = -8.41\ cm^{-1}$, and $D = 6.0\ cm^{-1}$ for *trans*-**3**. The ruffling of the porphyrin ring allows strong antiferromagnetic coupling between the porphyrin π-cation radical and the iron center, which is otherwise forbidden with planar macrocycles.[5d] The extensive π-conjugation between two porphyrin units of the bisporphyrin, through the bridging ethylene group, allows antiferromagnetic coupling between the two radical spins of the two porphyrin units although the cores are well separated and not cofacial enough to have any through space interactions.

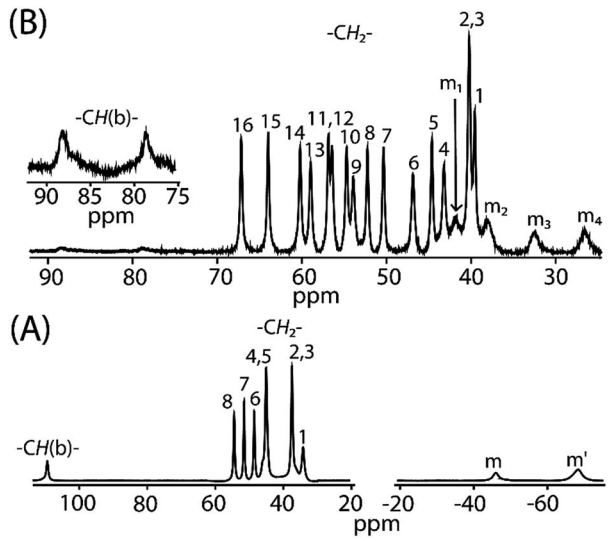

Fig. 12 ^{1}H NMR spectra (in $CDCl_3$ at 295 K) of (A) *cis*-**1** and (B) *trans*-**2**. Here, –C*H*(b)– marks the bridging protons and m, m′, m_1–m_4 represents *meso* proton signals.

^{1}H NMR

Fig. 12 compares the ^{1}H NMR spectra between *cis*-**1** and *trans*-**2**. For *trans*-**3** the signals are too broad to be detected. The ^{1}H NMR spectra of *cis*-**1** shows the presence of eight methylene proton resonances between 34 to 55 ppm, two upfield shifted *meso* signals at −68.9 and −46.2 ppm in 2 : 1 intensity ratio, and a highly downfield shifted bridging signal at 110 ppm. However, sixteen methylene and four *meso* signals were obtained upon two electron oxidation of *cis*-**1** to form *trans*-**2**, which confirms the presence of two inequivalent iron(III) centers as also evident from the X-ray structure and Mössbauer spectra of the complex in the solid state. The most conspicuous features in the ^{1}H NMR spectra of *trans*-**2** are the wide range of methylene resonances (39.5 to 67.1 ppm) and highly downfield shifted *meso* proton signals (at 26.5, 32.4, 37.9 and 41.8 ppm) which are attributed to the presence of porphyrin π-cation radicals and also to the increase in coordination number (from five to six).[20] Mulliken spin densities have also been calculated and reveal a negative spin density on the *meso* and bridging carbon atoms (Fig. S6†), hence the downfield shifts of the corresponding proton signals which also indicates the presence of the antiferromagnetic coupling of the iron spin with the $S = 1/2$ porphyrin radical as observed in the variable temperature magnetic measurements.[20a,b] Moreover, bridging protons are found at 78.6 and 88.3 ppm which are extremely broad due to the extensive delocalization of the radical through the bridging group as also evident in the alteration of the C20–C37 and C37–C37A bond lengths (*vide supra*). The temperature dependence of the proton signals follows the Curie law (Fig. S7†) which suggests the presence of a single spin state throughout the temperature range.

EPR

X-band EPR spectra have been recorded at 77 K for *trans*-**2** and *trans*-**3** both in solid and solution phases and Fig. 13 displays the experimental and simulated spectra while Table S2† lists the simulation parameters. Simulation of the spectra of *trans*-**2** yields $g_\perp = 5.470$ and $g_\parallel = 1.945$ which is consistent with admixed high spin iron(III) as also observed from the Mössbauer data and X-ray structure of the complex in the solid state. Trace B shows the EPR spectra of *trans*-**3** which is composed of two distinct features: a single isotropic line ($g = 2.016$) characteristic of an unresolved $^6S_1$ state indicating spin $S = 1/2$ and a $+1/2 \leftrightarrow -1/2$ transition, consistent with a $[FeCl_4]^-$ anion,[18b] and a second minor component with $g_\perp = 5.750$ and $g_\parallel = 1.942$, indicative of a high-spin iron(III). Moreover, the EPR signals of the 2e-oxidised complexes reported here are weak due to relatively weak intramolecular coupling between iron–radical (J_{Fe-r}) and radical–radical (J_{r-r}) spins (*vide supra*), although stronger coupling would result in no observable signals.

MauG is an enzyme unique in several respects. In heme-dependent enzymes, the two-electron oxidized intermediate

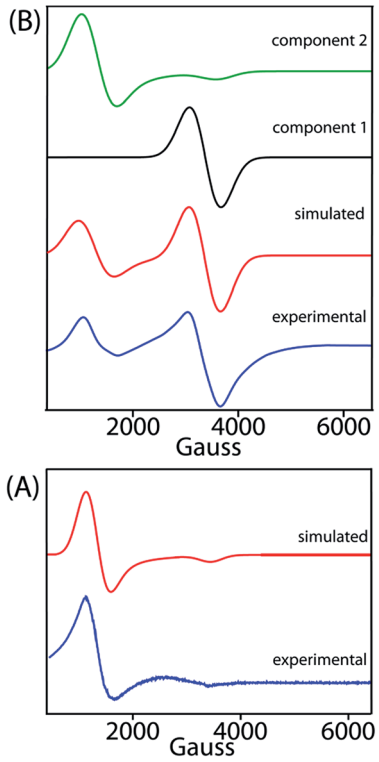

Fig. 13 X-band EPR spectra of (A) *trans*-**2** and (B) *trans*-**3** in CH_2Cl_2 (at 77 K). Blue and red lines represent experimental and simulated spectra, respectively. The black and green lines represent the two components used in the simulation of the EPR spectra of *trans*-**3**.

(compound I) consists of an Fe(IV) species coupled to an organic radical that is located on the porphyrin ring/axial ligand or a nearby amino acid residue (compound ES).[1–3] However, the two oxidizing equivalents derived from H_2O_2 are distributed within the diheme system as two positive charges, giving rise to the bis-Fe(IV) redox state in MauG.[8] This is electronically equivalent to two ferric hemes, each coupled with a porphyrin cation radical, a scenario resembling the binuclear dication diradical complex as observed in the 2e-oxidized complexes of *trans*-**2** and *trans*-**3** reported here. Although the spins and charges are delocalized throughout the diheme system and are stabilized *via* a series of possible charge resonance structures (responsible for the observed NIR band), the most stable form is a binuclear dication diradical complex which is found spectroscopically as the most stable conformer both in the solid state and in solution.

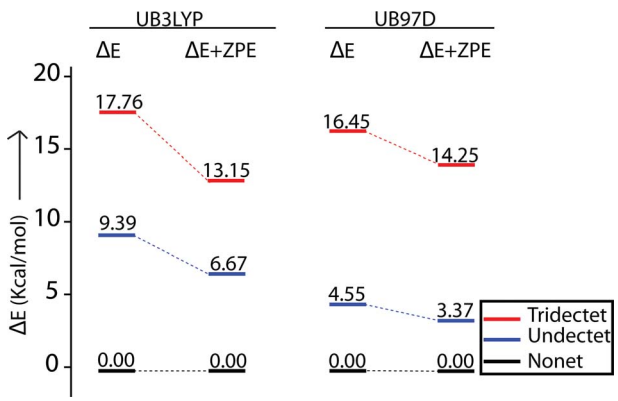

Fig. 14 Relative spin-state energies of nonet (9), undectet (11) and tridectet (13) states of *trans*-**2** as calculated using unrestricted B3LYP and B97D functionals in DFT. All the Δ*E* and Δ*E* + ZPE values are relative to nonet (9) state.

Molecular modeling

A series of DFT calculations have been carried out to get more insights into the electronic structure of the oxidized species. *Trans*-**2** has been optimized in three possible spin

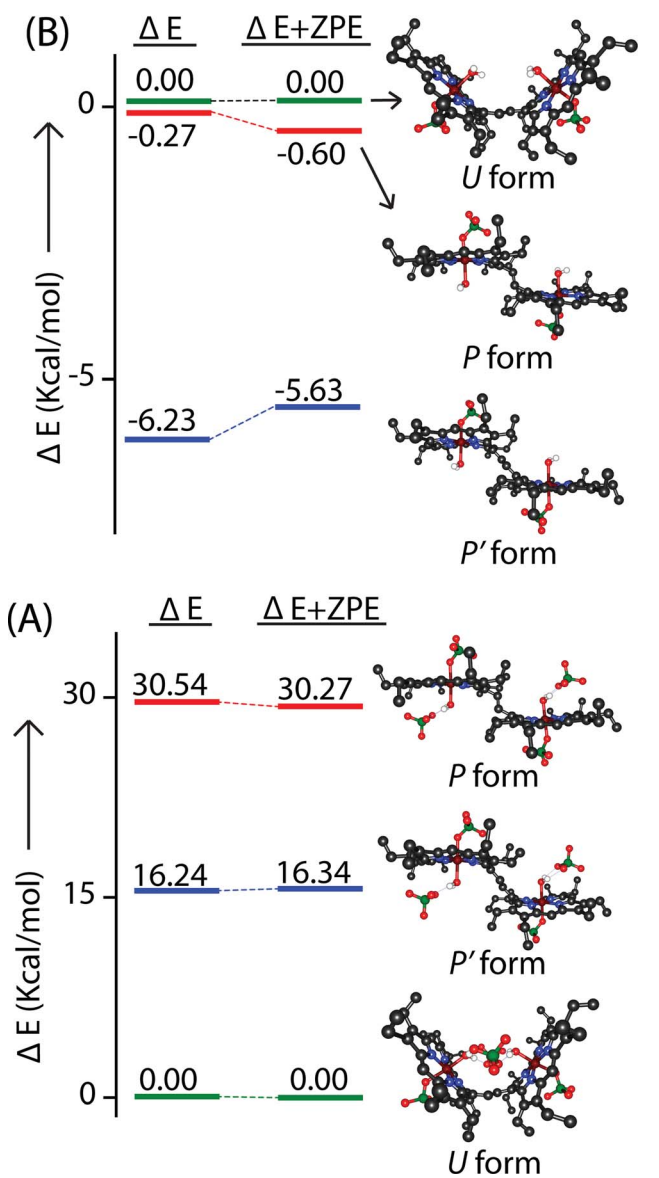

Fig. 15 Relative energies of the *U*, *P*, and *P*′ form of nonet (9) states of (A) *trans*-**2** and (B) *trans*-**2** (without counterion) as calculated using unrestricted B3LYP in DFT. All the Δ*E* and Δ*E* + ZPE values are relative to the *U* form.

multiplicities: nonet (9) state (considering antiferromagnetic interactions between the π-cation radical and the iron(III) spin), undectet (11) state (considering antiferromagnetic coupling between the two π-cation radical centers) and tridectet (13) state (considering ferromagnetic interactions between the cation radical and iron(III) spin). However, the interactions between the two iron(III) centers of *trans*-**2** in all these states have been considered to be ferromagnetic in nature. Since we are dealing with a large computational model, we have chosen to stick with a pure high-spin state ($S = 5/2$) for the iron(III) centers, although experimental data suggest a minor contribution from the intermediate spin ($S = 3/2$) in *trans*-**2**. Fig. S8 and S9† show the optimized geometries of *trans*-**2** with varying spin states in unrestricted B3LYP[21] and B97D[22] (includes dispersion correction) functional, while Fig. 14 schematically represents their relative energies. Clearly, the nonet state is energetically more stable than the undectet state, and the tridectet state is the least stable. This is also in good agreement with the experimental results.

In an attempt to find the probable reason behind such stabilization of the *U* form over the others, we have further optimized the molecule in different conformations, namely the *P*′ and *P* forms, both in the presence and absence of counterions. Fig. S10–S15† represent the optimized geometries while Fig. 15 shows the relative energies of different conformations both in the presence and absence of counterions. For *trans*-**2**, the *U* form is more stable than the *P*′ and *P* forms by 16.34 kcal mol^{-1} and 30.27 kcal mol^{-1}, respectively. However, in the absence of counterions, the *P*′ form becomes the most stable one, being 5.63 kcal mol^{-1} lower in energy than the *U*-form, while the *P*-form is similar (with a difference of −0.6 kcal mol^{-1}) in energy to the *U*-form. This proves that H-bonding interactions between the axial H_2O and the ClO_4^- counterion are responsible for the unusual stabilization of the *U* conformer which is otherwise strained. This is also evident in the stabilization of the *P*′ conformer for *trans*-**3** where there is no H-bonding interaction with the counterion ($FeCl_4^-$). Both the HOMO and the LUMO (Fig. 16 and S16†) of *trans*-**2** were found to have significant coefficients on the bridging ethylene group for the *U* and *P*′ forms, suggesting a substantial conjugation through the bridge, while the *P* form shows no such conjugation which is also in accord with the experiment. Although metallo-OEP radicals are known to have an a_{1u} type HOMO, *trans*-**2** is best described as a mixture of both a_{1u} and a_{2u} type orbitals (Fig. 16).[23] While the positions of infrared marker bands of porphyrin π-cation radicals are characteristics of an a_{1u}-type symmetry, the presence of a_{2u} type is clearly evident in the large shifts of the *meso* proton signals in the ^{1}H NMR (*vide supra*). Thus, computational studies clearly support the experimental observations.

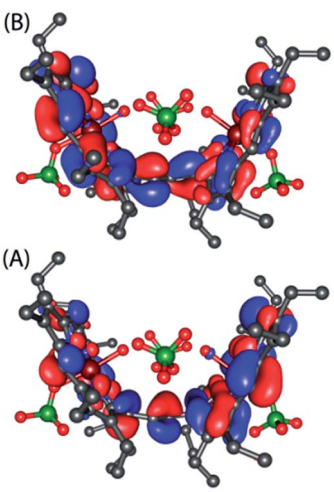

Fig. 16 (A) HOMO and (B) LUMO of *U* form of *trans*-**2** as obtained from the unrestricted B3LYP optimized geometry using nonet (9) state.

Summary

We have reported here the structural and spectroscopic evidence for two interacting Fe(III) porphyrin π-cation radicals that are covalently connected through an ethylene bridge and thus are too widely separated to have any through space interaction. 2e-oxidation of the diiron(III) porphyrin dimer leads to the conversion of the *cis* isomer to *trans* along with the stabilization of two unusual conformations (*U* and *P*′-type) which have widely different and distinct spectroscopic and geometric features and are different from the normal *trans* conformer (*P*-type). Through the bridging ethylene group, both porphyrin macrocycles exhibit notable conjugation resulting in effective coupling between iron and porphyrin radical spins of both rings. In fact, oxidation leads to a change in identity of the bridge which further highlights the key role played by the bridge in communicating the electronic properties between two rings. The conformers can be considered as a real supramolecule rather than two interacting discrete Fe(III) porphyrin π-cation radicals. DFT calculations further support the spin coupling model obtained from magnetic studies suggesting the nonet state of *trans*-**2** as the energetically favorable one. It also revealed that the extended π-conjugation and H-bonding interactions are the major factors in controlling the stability of the unusual conformers in the oxidized complexes.

Acknowledgements

This work is dedicated to Prof. Samaresh Mitra on the occasion of his 75th birthday.

We thank IIT Kanpur for providing all the facilities and support. The Council of Scientific and Industrial Research (CSIR), New Delhi, and Science and Engineering Research Board (SERB), India are gratefully acknowledged for financial support. D. S. and S. D. thank University Grant Commission (UGC), India and A. K. and S. B. thank the Council of Scientific and Industrial Research (CSIR), New Delhi for their fellowship.

References

1 (*a*) T. L. Poulos, *Chem. Rev.*, 2014, **114**, 3919–3962; (*b*) P. R. Ortiz de Montellano, in *Biocatalysis Based on Heme Peroxidases*, ed. E. Torres and M. Ayala, Springer, Berlin,

2010, pp. 79–107; (*c*) G. L. Berglund, G. H. Carlsson, A. T. Smith, H. Szöke, A. Henriksen and J. Hajdu, *Nature*, 2002, **417**, 463–468.

2 (*a*) M. Alfonso-Prieto, X. Biarnés, P. Vidossich and C. Rovira, *J. Am. Chem. Soc.*, 2009, **131**, 11751–11761; (*b*) P. Chelikania, I. Fitab and P. C. Loewen, *Cell. Mol. Life Sci.*, 2004, **61**, 192–208; (*c*) M. T. Green, *J. Am. Chem. Soc.*, 2001, **123**, 9218–9219.

3 (*a*) P. R. Ortiz de Montellano, *Cytochrome P450: structure, mechanism and biochemistry*, Plenum, Kluwer, New York, 3rd edn, 2005; (*b*) A. B. McQuarters, M. W. Wolf, A. P. Hunt and N. Lehnert, *Angew. Chem., Int. Ed.*, 2014, **53**, 4750–4752; (*c*) P. R. Ortiz de Montellano, *Chem. Rev.*, 2010, **110**, 932–948; (*d*) J. Rittle and M. T. Green, *Science*, 2010, **330**, 933–937; (*e*) I. G. Denisov, T. M. Makris, S. G. Sligar and I. Schlichting, *Chem. Rev.*, 2005, **105**, 2253–2277; (*f*) S. Shaik, D. Kumar, S. P. de Visser, A. Altun and W. Thiel, *Chem. Rev.*, 2005, **105**, 2279–2328; (*g*) B. Meunier, S. P. de Visser and S. Shaik, *Chem. Rev.*, 2004, **104**, 3947–3980; (*h*) L. Ji, A. S. Faponle, M. G. Quesne, M. A. Sainna, J. Zhang, A. Franke, D. Kumar, R. van Eldik, W. Liu and S. P. de Visser, *Chem.–Eur. J.*, 2015, **21**, 9083–9092.

4 (*a*) P. Jordan, P. Fromme, H. T. Witt, O. Klukas, W. Saenger and N. Krau, *Nature*, 2001, **411**, 909–917; (*b*) K. N. Ferreira, T. M. Iverson, K. Maghlaoui, J. Barber and S. Iwata, *Science*, 2004, **303**, 1831–1838; (*c*) Z. Liu, H. Yan, K. Wang, T. Kuang, J. Zhang, L. Gui, X. An and W. Chang, *Nature*, 2004, **428**, 287–292; (*d*) A. A. Pascal, Z. Liu, K. Broess, B. van Oort, H. van Amerongen, C. Wang, P. Horton, B. Robert, W. Chang and A. Ruban, *Nature*, 2005, **436**, 134–137; (*e*) B. Loll, J. Kern, W. Saenger, A. Zouni and J. Biesiadka, *Nature*, 2005, **438**, 1040–1044; (*f*) A. Amunts, O. Drory and N. Nelson, *Nature*, 2007, **447**, 58–63.

5 (*a*) M. Li, T. J. Neal, G. R. A. Wyllie, C. E. Schulz and W. R. Scheidt, *Inorg. Chem.*, 2010, **49**, 8078–8085; (*b*) T. J. Neal, S. J. Kang, I. Turowska-Tyrk, C. E. Schulz and W. R. Scheidt, *Inorg. Chem.*, 2000, **39**, 872–880; (*c*) S. Hu and T. G. Spiro, *J. Am. Chem. Soc.*, 1993, **115**, 12029–12034; (*d*) S. Nakashima, H. Ohya-Nishiguchi, N. Hirota, H. Fujii and I. Morishima, *Inorg. Chem.*, 1990, **29**, 5207–5211.

6 (*a*) M. Li, T. J. Neal, G. R. A. Wyllie, A. G. Oliver, C. E. Schulz and W. R. Scheidt, *Inorg. Chem.*, 2011, **50**, 9114–9121; (*b*) A. Takai, C. P. Gros, J. M. Barbe, R. Guilard and S. Fukuzumi, *Chem.–Eur. J.*, 2009, **15**, 3110–3122; (*c*) K. E. Brancato-Buentello, S.-J. Kang and W. R. Scheidt, *J. Am. Chem. Soc.*, 1997, **119**, 2839–2846; (*d*) W. R. Scheidt, K. E. Brancato-Buentello, H. Song, K. V. Reddy and B. Cheng, *Inorg. Chem.*, 1996, **35**, 7500–7507.

7 (*a*) L. M. R. Jensen, R. Sanishvili, V. L. Davidson and C. M. Wilmot, *Science*, 2010, **327**, 1392–1394; (*b*) Y. Wang, M. E. Graichen, A. Liu, A. R. Pearson, C. M. Wilmot and V. L. Davidson, *Biochemistry*, 2003, **42**, 7318–7325; (*c*) W. S. McIntire, D. E. Wemmer, A. Chistoserdov and M. E. Lidstrom, *Science*, 1991, **252**, 817–824; (*d*) Y. Ling, V. L. Davidson and Y. Zhang, *J. Phys. Chem. Lett.*, 2010, **1**, 2936–2939; (*e*) X. Li, M. Feng, Y. Wang, H. Tachikawa and V. L. Davidson, *Biochemistry*, 2006, **45**, 821–828.

8 (*a*) J. Geng, I. Davis and A. Liu, *Angew. Chem., Int. Ed.*, 2015, **54**, 3692–3696; (*b*) J. Geng, K. Dornevil, I. Davis and A. Liu, *Proc. Natl. Acad. Sci. U. S. A.*, 2013, **110**, 9639–9644; (*c*) X. Li, R. Fu, S. Lee, C. Krebs, V. L. Davidson and A. Liu, *Proc. Natl. Acad. Sci. U. S. A.*, 2008, **105**, 8597–8600.

9 (*a*) G. S. Pulcu, K. E. Frato, R. Gupta, H. R. Hsu, G. A. Levine, M. P. Hendrich and S. J. Elliott, *Biochemistry*, 2012, **51**, 974–985; (*b*) J. Seidel, M. Hoffmann, K. E. Ellis, A. Seidel, T. Spatzal, S. Gerhardt, S. J. Elliott and O. Einsle, *Biochemistry*, 2012, **51**, 2747–2756; (*c*) C. F. Becker, N. J. Watmough and S. J. Elliott, *Biochemistry*, 2009, **48**, 87–95; (*d*) G. W. Pettigrew, A. Echalier and S. R. Pauleta, *J. Inorg. Biochem.*, 2006, **100**, 551–567; (*e*) A. Echalier, C. F. Goodhew, G. W. Pettigrew and V. Fülöp, *Structure*, 2006, **14**, 107–117.

10 (*a*) M. Son, Y. M. Sung, S. Tokuji, N. Fukui, H. Yorimitsu, A. Osuka and D. Kim, *Chem. Commun.*, 2014, **50**, 3078–3080; (*b*) L. Rintoul, S. R. Harper and D. P. Arnold, *Phys. Chem. Chem. Phys.*, 2013, **15**, 18951–18964; (*c*) O. Locos, B. Bašić, J. C. McMurtrie, P. Jensen and D. P. Arnold, *Chem.–Eur. J.*, 2012, **18**, 5574–5588; (*d*) L. J. Esdaile, P. Jensen, J. C. McMurtrie and D. P. Arnold, *Angew. Chem., Int. Ed.*, 2007, **46**, 2090–2093; (*e*) M. J. Frampton, H. Akdas, A. R. Cowley, J. E. Rogers, J. E. Slagle, P. A. Fleitz, M. Drobizhev, A. Rebane and H. L. Anderson, *Org. Lett.*, 2005, **7**, 5365–5368; (*f*) M. Chachisvilis, V. S. Chirvony, A. M. Shulga, B. Källebring, S. Larsson and V. Sundström, *J. Phys. Chem.*, 1996, **100**, 13857–13866; (*g*) M. Chachisvilis, V. S. Chirvony, A. M. Shulga, B. Källebring, S. Larsson and V. Sundström, *J. Phys. Chem.*, 1996, **100**, 13867–13873; (*h*) V. S.-Y. Lin, S. G. DiMagno and M. J. Therien, *Science*, 1994, **264**, 1105–1111.

11 (*a*) D. Sil and S. P. Rath, *Dalton Trans.*, 2015, **44**, 16195–16211; (*b*) M. A. Sainna, D. Sil, D. Sahoo, B. Martin, S. P. Rath, P. Comba and S. P. de Visser, *Inorg. Chem.*, 2015, **54**, 1919–1930; (*c*) D. Sil, F. S. T. Khan and S. P. Rath, *Inorg. Chem.*, 2014, **53**, 11925–11936; (*d*) S. Bhowmik, S. Dey, D. Sahoo and S. P. Rath, *Chem.–Eur. J.*, 2013, **19**, 13732–13744; (*e*) S. K. Ghosh, S. Bhowmik, D. Sil and S. P. Rath, *Chem.–Eur. J.*, 2013, **19**, 17846–17859; (*f*) S. Bhowmik, S. K. Ghosh and S. P. Rath, *Chem.–Eur. J.*, 2012, **18**, 13025–13037; (*g*) S. Bhowmik, S. K. Ghosh and S. P. Rath, *Chem. Commun.*, 2011, **47**, 4790–4792; (*h*) S. Bhowmik, D. Sil, R. Patra and S. P. Rath, *J. Chem. Sci.*, 2011, **123**, 827–837; (*i*) S. K. Ghosh and S. P. Rath, *J. Am. Chem. Soc.*, 2010, **132**, 17983–17985; (*j*) S. K. Ghosh, R. Patra and S. P. Rath, *Inorg. Chim. Acta*, 2010, **363**, 2791–2799; (*k*) S. K. Ghosh, R. Patra and S. P. Rath, *Inorg. Chem.*, 2010, **49**, 3449–3460; (*l*) S. K. Ghosh, R. Patra and S. P. Rath, *Inorg. Chem.*, 2008, **47**, 10196–10198; (*m*) S. Dey and S. P. Rath, *Dalton Trans.*, 2014, **43**, 2301–2314.

12 T. E. Clement, D. J. Nurco and K. M. Smith, *Inorg. Chem.*, 1998, **37**, 1150–1160.

13 (*a*) S. V. Lindeman, S. V. Rosokha, D. L. Sun and J. K. Kochi, *J. Am. Chem. Soc.*, 2002, **124**, 843–855; (*b*) S. V. Rosokha, D. L. Sun and J. K. Kochi, *J. Phys. Chem. A*, 2002, **106**, 2283–2292; (*c*) D. L. Sun, S. V. Rosokha, S. V. Lindeman

and J. K. Kochi, *J. Am. Chem. Soc.*, 2003, **125**, 15950–15963; (*d*) J. M. Lü, S. V. Rosokha and J. K. Kochi, *J. Am. Chem. Soc.*, 2003, **125**, 12161–12171.

14 N. J. Hill, W. Levason, M. C. Popham, G. Reid and M. Webster, *Polyhedron*, 2002, **21**, 445–455.

15 (*a*) R. Weiss, A. Gold and J. Terner, *Chem. Rev.*, 2006, **106**, 2550–2579; (*b*) M. Nakamura, *Coord. Chem. Rev.*, 2006, **250**, 2271–2294.

16 (*a*) D. Sahoo, M. G. Quesne, S. P. de Visser and S. P. Rath, *Angew. Chem., Int. Ed.*, 2015, **54**, 4796–4800; (*b*) R. Patra, S. Bhowmik, S. K. Ghosh and S. P. Rath, *Dalton Trans.*, 2010, **39**, 5795–5806; (*c*) R. Patra, A. Chaudhary, S. K. Ghosh and S. P. Rath, *Inorg. Chem.*, 2010, **49**, 2057–2067; (*d*) R. Patra and S. P. Rath, *Inorg. Chem. Commun.*, 2009, **12**, 515–519; (*e*) R. Patra, A. Chaudhary, S. K. Ghosh and S. P. Rath, *Inorg. Chem.*, 2008, **47**, 8324–8335; (*f*) D. Sahoo and S. P. Rath, *Chem. Commun.*, 2015, **51**, 16790–16793.

17 C. A. Reed and F. Guiset, *J. Am. Chem. Soc.*, 1996, **118**, 3281–3282.

18 (*a*) D. Wyrzykowski, A. Pattek-Janczyk, T. Maniecki, K. Zaremba and Z. Warnke, *Thermochim. Acta*, 2006, **443**, 72–77; (*b*) D. Wyrzykowski, R. Kruszyński, J. Kłak, J. Mroziński and Z. Warnke, *Inorg. Chim. Acta*, 2007, **360**, 3354–3360.

19 N. F. Chilton, R. P. Anderson, L. D. Turner, A. Soncini and K. S. Murray, *J. Comput. Chem.*, 2013, **34**, 1164–1175.

20 (*a*) A. Ikezaki, Y. Ohgo and M. Nakamura, *Coord. Chem. Rev.*, 2009, **253**, 2056–2069; (*b*) S. Kouno, A. Ikezaki, T. Ikeue and M. Nakamura, *J. Biol. Inorg. Chem.*, 2011, **105**, 718–721; (*c*) F. A. Walker, in *Handbook of Porphyrin Science*, ed. K. M. Kadish, K. M. Smith and R. Guilard, World Scientific, Singapore, 2010, vol. 6, pp. 1–137.

21 (*a*) A. D. Becke, *J. Chem. Phys.*, 1993, **98**, 5648–5652; (*b*) C. Lee, W. Yang and R. G. Parr, *Phys. Rev. B: Condens. Matter Mater. Phys.*, 1988, **37**, 785–789; (*c*) P. J. Stevens, F. J. Devlin, C. F. Chabalowski and M. Frisch, *J. Phys. Chem.*, 1994, **98**, 11623–11627.

22 S. J. Grimme, *Comput. Chem.*, 2006, **27**, 1787–1799.

23 (*a*) T. Vangberg, R. Lie and A. Ghosh, *J. Am. Chem. Soc.*, 2002, **124**, 8122–8130; (*b*) H. Hirao, S. Shaik and P. M. Kozlowski, *J. Phys. Chem. A*, 2006, **110**, 6091–6099; (*c*) R. J. Cheng, P. Y. Chen, T. Lovell, T. Liu, L. Noodleman and D. A. Case, *J. Am. Chem. Soc.*, 2003, **125**, 6774–6783.